International Journal of Engineering

Journal Homepage: www.ije.ir

Fuzzy Logic Control of Maximum Power Point Tracking Controller in an Autonomous Hybrid Power Generation System by Extended Kalman Filter for Battery State of Charge Estimation

K. Sahel Hanane[a], L. Abderrazak*[b], R. Adlene[b], A. Mohamed[a], K. Mohamed[b]

[a] *Mechanical Engineering Department, Automatic Laboratory, University of 20 August 1955, Skikda, Algeria*
[b] *Electrical Engineering Department, Automatic Laboratory, University of 20 August 1955, Skikda, Algeria*

PAPER INFO

Paper history:
Received 07 April 2022
Received in revised form 04 November 2022
Accepted 05 November 2022

Keywords:
Management
Hybrid Photovoltaic System
Stand-alone
DC-DC Converter
State of Charge Estimation
Extended Kalman Filter

ABSTRACT

Autonomous power generation systems are designed to operate independently from the public power grid. Batteries constitute the important element in stand-alone PV system. They are used to store electricity produced by solar energy at overnight or for emergency use during the non-constant load demand. This paper has three major parts.The first pertains the design of an intelligent method for maximum power point tracking based on fuzzy logic controller to improve the efficiency of a standalone solar energy system. The second part describes the battery state of charge (SOC). The proposed model, which better reflects the real SOC response of the lithium battery, is constructed by using the extended Kalman Filter (EKF) states estimator. This proposed method can be considered as a more accurate and reliable method to estimate the battery state of charge. The third part integrates a management system for the above two renewable energy sources. The performance of the proposed management system by using a fuzzy logic controller based maximum power point tracking FLC-MPPT and the EKF estimator have been simulated in Matlab/Simulink at different solar irradiation and temperature for a given no constant load energy request.

***doi**: 10.5829/ije.2023.36.02b.02*

NOMENCLATURE

q	Electron Charge	v, w	zero-mean white Gaussian
α	Duty cycle	$A_k = \frac{\partial f(x,u)}{\partial x}\Big\|_{x(t),u(t)}$	Linearized System Matrix
x	State variable	$C_k = \frac{\partial f(x,u)}{\partial x}\Big\|_{x(t),u(t)}$	Linearized Output Matrix
u	Control variable	R_{L1} & R_{L2}	Load Resistors
$K_k = P_{k/k-1}C_d^T\left[C_d P_{k/k-1} C_d^T + \Sigma_v\right]^{-1}$	Kalman gain matrix	$P_{k/k-1} = A_d P_{k-1/k-1} A_d^T + \Sigma_w$	Error covariance time update

1. INTRODUCTION

In recent years, solar energy, in particular photovoltaic energy, has seen a significant development as an alternative to meet energy demands, especially in desert areas or for reasons of environmental concern and the fall in the prices of photovoltaic modules [1].

For this purpose, photovoltaic (PV) panels, which are the main technology for converting solar energy into electrical energy, can be installed as stand-alone systems to produce electrical energy in certain isolated areas or be connected to supply the electrical network. Because solar energy is instantaneous and unstable by nature, the PV energy system works in conjunction with storage batteries to provide continuous and stable power in the configuration of hybrid stand-alone power systems photovoltaic generator (GPV)/ batteries. Battery storage can be considered an auxiliary power source to reduce the

*Corresponding Author Institutional Email: a.lachouri@univ-skikda.dz (L. Abderrazak)

Please cite this article as: K. Sahel Hanane, L. Abderrazak, R. Adlene, A. Mohamed, K. Mohamed, Fuzzy Logic Control of Maximum Power Point Tracking Controller in an Autonomous Hybrid Power Generation System by Extended Kalman Filter for Battery State of Charge Estimation, ***International Journal of Engineering, Transactions B: Applications***, Vol. 36, No. 02, (2023), 199-214

risk of PV's irregular power supply, and always ensure the satisfaction of demand [2]. Indeed, to enhance the effectiveness of the PV generation system, DC/DC converters are always used to follow up on the maximal power extracted (MPP) from the PV array system and adapt the connection with an electrical network or battery bank to adjust the power flow route and optimize the whole system performance [3]. In order to retrieve the maximum power delivered by the PV generator, researchers are working on improving MPPT algorithms [4]. In the literature, several algorithms and techniques are developed for calculating the MPPT, such as the perturbation and observation (P&O) algorithm, the incremental conductance algorithm (InCond), the ripple correlation control algorithm (RCC), the fractional voltage/current MPPT, the fuzzy logic controller MPPT algorithm, and the neural network (NN)-based MPPT control [5]. However, the most famous MPPT is the fuzzy logic controller, which is widely adopted because it is the simplest and most robust method among all MPPT ones. The FLC method can be introduced also in other contexts for searching the maximum (or minimum) of a function [6]. Other than an MPPT controller, inverters for PV or grid-connected or stand-alone AC systems, DC/DC converters (buck, boost, buck-boost, Cuk, single-ended primary inductance converter SEPIC etc.) and storage elements such as electrical batteries, which are used to improve the PV efficiency and regulate the output voltage [7].

Hybrid power systems (HPS) based on renewable energy (RE) are a good alternative for conventional systems to guarantee the continuity of electricity supply to customers. In general, batteries are the most common in this context. Many companies are interested in the management and storage of solar energy and providing more intelligent solutions for the solar energy markets, whether for home use or for commercial and industrial use. However, to meet this requirement, we can find that batteries constitute the most attractive energy storage systems because of their high efficiency and low pollution. However, the batteries must be protected against overcharging and deep discharging. This requires continuous monitoring for both the battery state of charge and the energy produced by the photovoltaic panels [8]. Therefore, the battery State of Charge (SOC) which used to estimate its remaining stored charge, is a very important parameter to establish a control strategy [9]. In this context, real-time tracking with an accurate estimate of its SOC can not only protect the battery from overcharging and over discharging and improve its life duration but also allow the applications to make rational control strategies in order to ensure the reliability of the power production system and optimize energy management [10].

There are many types of batteries currently used in the industry: lead-acid batteries, Ni-MH, Ni-Cd and Li-ion batteries. All these batteries have chemical energy storage that cannot be directly accessed and measured. In the literature, evaluation of SOC is essentially based on two methods, physical and electrical:

A. Physical methods: These methods are based on the observation of chemical and physical changes occurring in the battery during charging or discharging in operating mode. Among these methods, one involves measuring the gravity (or specific gravity) of the electrolyte.

B. Electrical methods: These methods are applicable to the majority of batteries. They are calculated from the measurements of the electrical parameters such as the voltage, the current, internal resistance, and impedance. Among these methods: method of charge counting or current integration, Fuzzy logic and ANN-based methods, and recently the Extend Kalman Filter (EKF).

This work presents three main contributions. The first contribution consists of the design of an intelligent method for maximum power point tracking based on fuzzy logic controllers. The second part describes the battery state of charge (SOC). The proposed model, which better reflects the real SOC response of the lithium battery, is constructed by using the extended Kalman Filter (EKF) states estimator realizing a software sensor for the measurement of the battery SOC. The advantage of such a method is that the SOC is optimally estimated even in the presence of wideband measurement noise affecting the system [11]. The paper is structured as follows: section 2 is devoted to the modeling of PV systems. A brief introduction to the control scheme is presented in section 3. Section 4 introduces an EKF-based SOC estimator for the developed model, and the simulation results are provided in section 5.

2. DESCRIPTION OF THE SYSTEM

A stand-alone alternative energy system consists of two or more energy sources, at least one of which is renewable [12]. Solar is a promising power generating source, but it depends on climatic conditions and geographical areas [13]. Generally, the residential PV-battery backup system consisted of a PV generator for the conversion of the solar irradiance to electrical power, deep-cycle flooded lead acid batteries for the storage of the electrical energy, Pulse Width Modulation (PWM) charge controller to regulate the charging operating mode of the battery bank. Also, a power converter is able to operate in two modes: DC/AC and AC/DC conversion. Figure 1 shows a schematic overview of a typical PV/battery Renewable Energy Hybrid System (REHS).

In this section, the PV generator and the storage battery are coupled with the inverter and connected to an AC bus system, which supplies directly the load. In such systems, the battery can be considered as the main source in the case, for instance, of insufficient PV production.

Furthermore, the PV power production has to be exploited with the highest efficiency. Therefore, it is necessary for an operation strategy to design the optimal economic solution for solving this problem. On another side, the capacity of battery has to be large enough to be charged from the power excess provided by the PV generator to cover the power deficit.

2. 1. PV Model In simulations, the literature reveals methods of modeling solar cells, with a major difference between using a single diode solar model or a double diode solar model. They display real system actions with the inclusion of losses [12]. In this paper, a single diode model is used. This model is characterized by its electric diagram, which is illustrated in Figure 2. The power source models the conversion of solar energy into electricity, the resistance shunt reflects the surface quality of the cell periphery, the resistance series refers to the different contact and interaction resistances performed on the cell, and the diode in the PN junction parallel models [13].

The current expression for equivalent solar model is given by Equation (1).

$$I = I_L - I_0\left(e^{\frac{q(V+I\cdot R_S)}{n\cdot k\cdot T}} - 1\right) - \frac{V+I\cdot R_S}{R_{SH}} \quad (1)$$

Generally, for modules in a PV system that are connected in arrays, the cell array contains Np parallel branches, each with Ns modules in series. The total current output can be deduced as follows from Equation (2) [14].

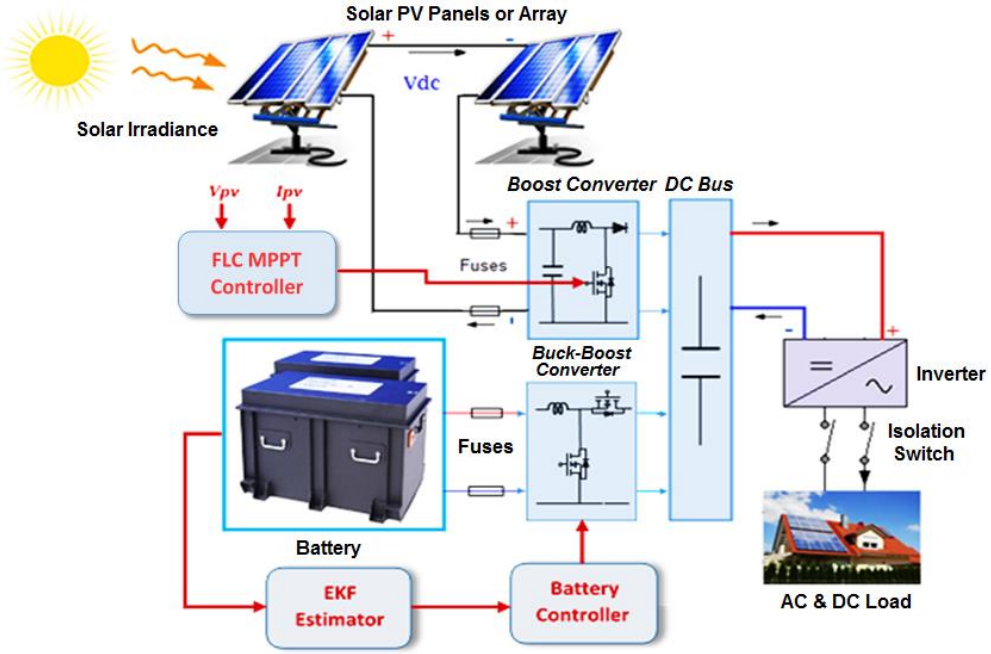

Figure 1. Schematic illustrating the studied REHS configuration

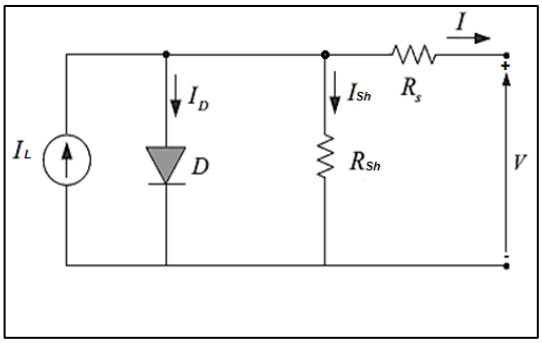

Figure 2. Equivalent Model of Single Diode Solar cell [15]

$$I = N_P\cdot I_L - N_P\cdot I_0\left(e^{\frac{q(V+(N_S/N_P)I\cdot R_S)}{n\cdot k\cdot T\cdot N_S}} - 1\right) - \frac{V+(N_S/N_P)I\cdot R_S}{(N_S/N_P)R_{SH}} \quad (2)$$

where:

- I: is the solar array output current (A).
- I_0: is the cell reverse saturation current (A).
- I_L: is the photo-generated current (A).
- V: is the solar panel output voltage (V).
- q: is the electron charge 1.602*10¯19 C.
- k: is the Boltzmann constant 1.381* 10¯²³ J/K.
- n: is the p-n junction ideality factor.
- T: is the temperature (K).

2. 2. DC/DC Converter The boost converter is used where a controlled average voltage is required by converting a DC voltage (V_{in}) to another DC voltage (V_0). As shown in Figure 3, it is comprised of a DC input voltage source V_{in}, boost inductor L, controlled switch (MOSFET), diode D, filter capacitor C, and load resistance R. When the switch S is in the on state, the boost inductor stores energy from the PV panel and the current increases linearly. The diode D is reverse biased at the time. However, if the switch S is turned off, the energy stored in the inductor is released through the diode to the input RC circuit. As the name of the converter suggests, the PV panel voltage is added to the inductor voltage (discharge state) to make the output voltage always greater than the input voltage [16].

This converter is modelled as follow [17]:

$$V_0 = \frac{V_{in}}{1-\alpha} \tag{3}$$

$$I_0 = I(1-\alpha) \tag{4}$$

where, α, V_{in} and I, V_0 and I_0 are respectively the duty cycle, PV input voltage, and current, and the output voltage and current of the boost converter.

2. 3. Modeling of Battery The battery is an important element of a stand-alone PV system. The equivalent circuit illustrated in Figure 4 gives the model of the lithium battery. The capacitances C_c and C_{cs} represent the battery storage capacity and the diffusion effects. The resistances R_i and R_t represent the internal and the polarization resistances respectively. The voltages across the bulk capacitor and the surface one are denoted by V_{cb} and V_{cs}. The terminal voltage and current are denoted by V_0 and I, respectivley [18]. For simplicity, the model equations can thus be characterized by the model, which is shown in Figure 4.

$$\dot{V}_{cb} = \frac{I}{C_{cb}} \tag{5}$$

$$\dot{V}_{cs} = \frac{1}{R_t C_{cs}} V_{cs} + \frac{1}{C_{cs}} I \tag{6}$$

$$V_0 = V_{cb} + V_{cs} + IR_i \tag{7}$$

It seems that the relationship between open circuit terminal voltage (OCV) and State of Charge SOC is only

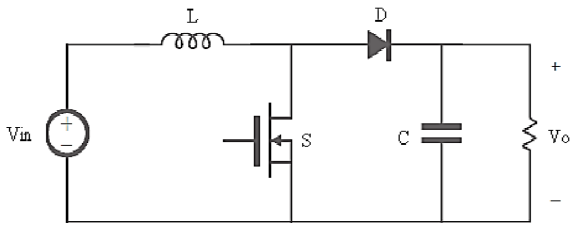

Figure 3. DC-DC Boost converter

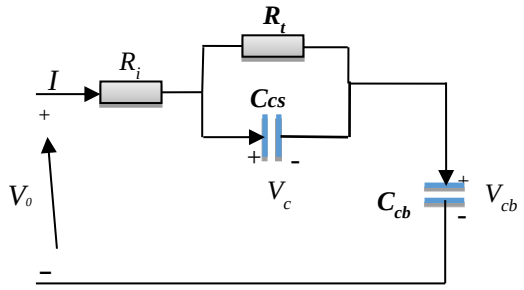

Figure 4. Equivalent circuit model for a lithium battery

piecewisely linear and static [19], one can define:

$$V_{cb} = kSoc + d \tag{8}$$

where k and d ≠ 0, (k and d are not constants and vary with battery SOC and the ambient temperature). Here, SOC represents the battery's State Of Charge. By substituting Equation (8) into Equation (5) ~ Equation (7), the equations describing the battery characteristics can be defined as:

$$\begin{bmatrix} \dot{Soc} \\ \dot{V}_{cs} \end{bmatrix} = \begin{bmatrix} \frac{I}{kC_{cb}} \\ -\frac{1}{R_t C_{cs}} V_{cs} + \frac{1}{C_{cs}} I \end{bmatrix} \tag{9}$$

$$V_0 = kSoc + V_{cs} + IR_i + d \tag{10}$$

3. CONTROL STRATEGIES

The literature has suggested several MPPT techniques to improve MPP algorithms that have been published, such as: P&O MPPT algorithm, Fractional Open-Circuit Voltage-Based MPPT, Incremental Conductance Based MPPT Technique, Fuzzy Logic Control Based MPPT, Neural Network Based MPP. Out of which, due to several advantages like fast operation, simple implementation, Fuzzy Logic Control Based MPPT is preferred [20-22].

3. 1. Fuzzy MPPT Control The MPPT fuzzy logic controller has been developed to extract the maximum solar energy by forcing the PV panel to operate at its maximum power point (MPP). This control is considered a crucial element for improving the efficiency of the PV system [23]. Fuzzy control is a method that allows the construction of nonlinear controllers from heuristic information that comes from the knowledge of an expert. In the MPPT configuration, Fuzzy Logic Controller (FLC) is used to determine the duty cycle of the DC-DC boost converter. In this study, the fuzzy logic controller was developed with two inputs and one output functions such as PV voltage, PV current, and duty cycle of the PV boost converter. Figure 5 shows the diagram of the FLC MPPT algorithm. The power produced by the

PV panels is calculated from the measured values of the current and voltage sensors [24]. The main parts of the FLC include: fuzzification, system inference, rule base, and defuzzification.

The fuzzy logic controller has been developed with two inputs and one output function, such as, dV_{pv}, dP_{pv} and duty cycle of the PV boost converter, as shown in Figure 6(a). The fuzzy dV_{pv} input membership function is classified into seven ranges, namely negative dV_{pv}, negative medium dV_{pv}, negative small dV_{pv}, zero dV_{pv}, positive small dV_{pv}, positive medium dV_{pv} and positive dV_{pv} as presented in Figure 6(b). The fuzzy PV dP_{pv} input membership function is classified into seven ranges, namely negative dP_{pv}, negative medium dP_{pv}, negative small dP_{pv}, zero dP_{pv}, positive small dP_{pv}, positive medium dP_{pv} and positive dP_{pv} as presented in Figure 6(c). The fuzzy duty cycle output membership function is classified into seven ranges that are negative Duty Cycle, negative medium Duty Cycle, negative small Duty Cycle, zero Duty Cycle, positive small Duty Cycle, positive medium Duty Cycle and positive Duty Cycle as presented in Figure 6(d). The fuzzy rules surface waveform presented in Figure 6(e).

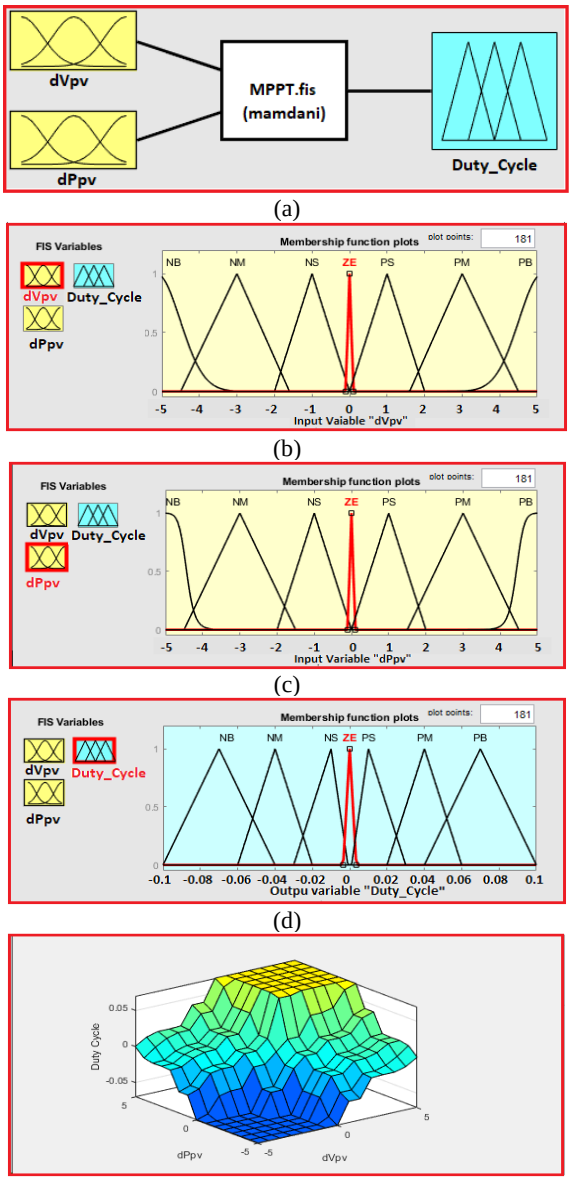

Figure 6. (a) Design of Fuzzy Controller for DC-DC converter (b) Input dV_{pv} Membership function (c) Input dP_{pv} Membership function, (d) Output Duty Cycle Membership function and (e) The fuzzy rules surface waveform

3. 2. Battery Charge Controller Based on simulation work done for a stand-alone PV system, a strategy for ON/OFF-switching control signals can be generated through a PID-type controller where the battery and the PV generator never simultaneously power the load. When the energy produced by the PV is not enough to meet the load demand, the secondary power supply (battery) takes over and supplies the load. This control strategy aims to adjust the phase between the system bus voltage (Vdc) and the battery voltage according to the state of charge (BAT_SOC). Figure 7(a) shows the ON/OFF-switching set points (or thresholds) for the battery and PV panel power contributions. When the power produced by the solar panels falls below the load demand, or the threshold, the battery is switched ON and kept on until BAT_SOC falls below the threshold. The two variables S1 and S2 are used to put the battery either in charging mode or in energy source mode according to Table 1.

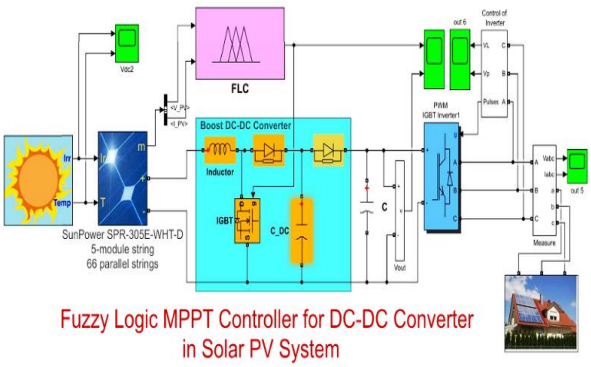

Figure 5. Fuzzy based MPPT controller simulation model for PV system Design of Fuzzy Logic Controller

The battery's operating mode is directly related to the DC-DC converter's functioning. In the case that the GPV energy production is insufficient, the battery takes over as an emergency power supply. Switching between the PV source and the battery is ensured by the gate control output, provided by a PI regulator Figure 7(b).

TABLE 1. Battery operating mode

S2	S1	Operating mode
0	0	Disconnected
0	1	Source
1	0	Loading
1	1	Disconnected

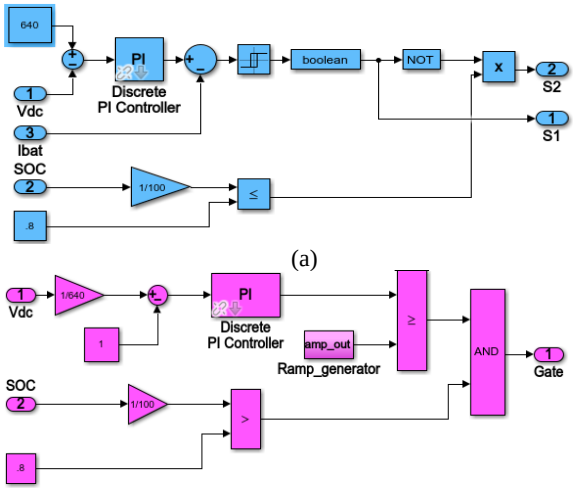

Figure 7. (a) Battery/electrolyzer Controller (b) PI Controller for Switching between the PV source and the battery

4. EKF-BASED SOC ESTIMATION

The EKF considers the noise characteristics of the current and voltage sensors, and effectively overcomes the effect of random errors. There exist several alternatives to the Kalman filter, depending to whether the mathematical model is linear, nonlinear, discrete or continuous. In this work, the battery is the dynamic model, and the state of charge constitutes the state variable to estimate. If the model is nonlinear, then we may use a linearization process at every time step to approximate the nonlinear system with a linear time varying (LTV) system. This LTV system is then implemented by Kalman filter, resulting in an Extended Kalman Filter (EKF) on the true nonlinear system. Note that although EKF effectiveness has been validated in many works [10, 25-27]. In this study, the EKF, based on dynamic equations, is used to estimate the battery state of charge [28] Figure 7.

The nonlinear system is presented as follows:

$$\dot{x}(t) = f(x,u) + w \tag{11}$$

$$y(t) = \mathrm{g}(x,u) + v \tag{12}$$

where, w and v are zero-mean white Gaussian stochastic processes with covariance matrices $\Sigma_w$and Σ_v respectively. Now, $f(x,u)$ is a nonlinear dynamics function and $g(x,u)$ is a nonlinear measurement function. The input is expressed as $u(t) = I$ and the output is $y = V_0$.

$$f(x,u) = \begin{bmatrix} \frac{u}{kC_{cb}} \\ -\frac{1}{R_t C_{cs}} x_2 + \frac{1}{C_{cs}} u \end{bmatrix} \tag{13}$$

$$\mathrm{g}(x,u) = kx_1 + x_2 + R_i u + d \tag{14}$$

At each time step, $f(x,u)$ and $g(x,u)$ are linearized by a first-order Taylor-series expansion. The linearized model is:

$$\delta\dot{x} = A_k \delta x + B_k \delta u \tag{15}$$

$$y = C_k \delta x + D_k \delta u \tag{16}$$

where:

$$A_k = \left.\frac{\partial f(x,u)}{\partial x}\right|_{x(t),u(t)} = \begin{bmatrix} 0 & 0 \\ 0 & -\frac{1}{R_t C_{cs}} \end{bmatrix}$$

$$B_k = \left.\frac{\partial f(x,u)}{\partial u}\right|_{x(t),u(t)} = \begin{bmatrix} \frac{1}{kC_{cs}} & \frac{1}{C_{cs}} \end{bmatrix}$$

$$C_k = \left.\frac{\partial f(x,u)}{\partial x}\right|_{x(t),u(t)} = [k \quad 1]$$

and $$D_k = \left.\frac{\partial g(x,u)}{\partial x}\right|_{x(t),u(t)} = R_i$$

The model represented by Equations (15)-(16) can be discretized as follows:

$$x_{k+1} = A_d x_k + B_d u_k \tag{17}$$

$$y_{k+1} = C_d x_k + D_d u_k \tag{18}$$

where:

$A_d \approx E + T_s A_k$,

$B_d \approx T_s B_k$,

$C_d \approx C_k$, and $D_d \approx D_k$, E is the unit matrix and T_s is the sampling period.

The algorithm of the EKF has three distinct phases: *Initialization, Prediction and upgraded* [28]:

Initialization: for k = 0, given the initial state values x_0, covariance matrix P, noise variance Σ_w and Σ_v.

Prediction: The step of prediction consists to using the state estimated of the previous moment to calculate an estimate of the current state.

The state estimate update:

$$\bar{x}_{k/k-1} = f\left(\bar{x}_{k-1/k-1}, u_{k-1}\right)$$

Error covariance time update:

$$P_{k/k-1} = A_d P_{k-1/k-1} A_d^T + \Sigma_w$$

Upgraded and correction: In this step, the current measurements are used to correct the state predicted to obtain a more precise estimate of the state.

Kalman gain matrix:

$$K_k = P_{k/k-1} C_d^T \left[C_d P_{k/k-1} C_d^T + \Sigma_v\right]^{-1}$$

State estimate measurement update:

$$\bar{x}_{k/k} = \bar{x}_{k/k-1} + K_k\left[y_k - \mathrm{g}\left(\bar{x}_{k/k-1}, I_k\right)\right]$$

Error covariance measurement update:

$$P_{k/k} = (E - K_k C_d) P_{k/k-1}$$

5. MATLAB/SIMULINK SIMULATION AND RESULTS

The solar panel model is made in *Matlab/Simulink* software, the model is simulated under STC, and the *I–V* and *P–V* characteristics are presented in Figure 8. These curves change depending on the temperature and solar irradiance variation Figure 9.

Simulation is the simplest and most efficient technique used today for the evaluation of engineering solutions. The MATLAB-SIMULINK model was designed, as depicted in Figure 9, to explore the performance of the integrated PV/Battery/AC & DC Load system and the control strategy. However, the components of the proposed stand-alone PV system are: The solar panels and storage batteries are connected to the DC bus by a DC/DC boost converter and DC/DC buck-boost converter consecutively. Then we find a three-phase inverter that is supervised by its own controller and it is used to convert from DC to AC voltage. Finally, two loads are connected / disconnected to the AC voltage side by the inverter controller, with Load 1 representing the critical one and Load 2 represents the less priority loads. The conventional fuzzy logic MPPT controller, is proposed and the calculation of the SOC status is evaluated by EKF observer. The PV module considered in the simulation is the Array type: SunPower SPR-305E-WHT-D (with a capacity of 100 kW); 5 series modules; 66 parallel strings in which the model parameters are given in Table 2.

A Stand-alone system involves no interaction with a utility grid. Many scenarios are considered to simulate the autonomous hybrid power system with local load variations. Firstly, we consider a constant temperature with varying irradiation and secondly a constant irradiance with varying temperature applied to the solar panel SunPower SPR-305E-WHT-D. For the 100 kW solar array block, we used 330 SunPower SPR-305E-WHT-D modules, connected in a combination of 66 cells in-parallel by 5 cells in-series. A series connection of cells results in higher voltages, while a parallel connection results in higher current. This array generates 100.7 kW at an irradiance of 1 kW/m^2 at a temperature of 25°C. Its MPP voltage varies approximately from 250.2 V to 296.6 V up to given environmental conditions. The DC-DC Converter operates at a switching frequency of 5 kHz and provides an output at 640 V DC. The DC link

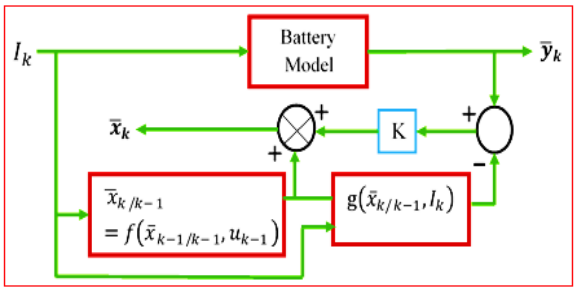

Figure 8. Structure of the Extended Kalman Filter

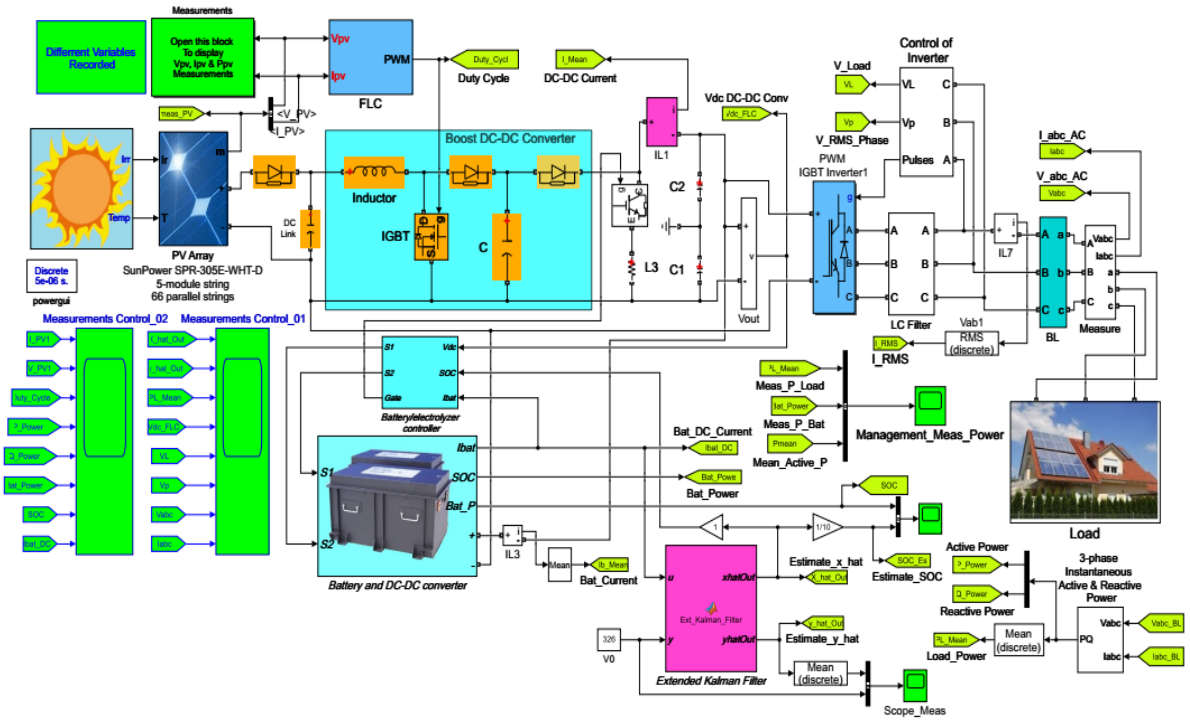

Figure 9. Simulink model of proposed control of the system

capacitors C1 and C2 play a damping role in order to maintain the stability of the MPPT during these transitory disturbances. This aspect is important because this ripple is directly perceived as electrical pollution at the output voltage of the PV module. By making step variations in the solar radiation S and the temperature T, the proposed power generation system of Figure 7 provided the I–V and P–V characteristics as shown in Figure 8. Hence, as shown, the sampling time T_s is 50 µs and the simulated data are in accordance with the characteristics mentioned in Table 2.

The DC link capacitors C1 and C2 play a damping role in order to maintain the stability of the MPPT during these transitory disturbances. This aspect is important because this ripple is directly perceived as electrical pollution at the output voltage of the PV module. By making step variations in the solar radiation S and the temperature T, the proposed power generation system of Figure 9 provided the I–V and the P–V characteristics as shown in Figure 10. Hence, as shown, the sampling time T_s is 50 µs and the simulated data are in accordance with the characteristics mentioned in Table 2.

5. 1. Effects of Changing Irradiance As the irradiance increases short circuit current also increases along with the open circuit voltage. Because of both increasing of V and I, the P_{max} is also increases according the irradiance.

Case Study 01: Irradiance and Temperature variation
For the first case study applied to the PV array type SunPower SPR-305E-WHT-D, the supervisory control considers the forecast energy demand of the end-users and makes instantaneous decisions about stand-alone energy production. The main goal of stand-alone system management is to satisfy the loads energy needs.

TABLE 2. PV module M/s SunPower SPR-305E-WHT-D Paramaters at STC (25°C & 1000W/m^2)

Designation	Value
Parallel String	66
Series-connected modules per string	5
No. of cells per module	96
Number not of modules	330
PV module power	305.226W
Isc of PV array	5.96 A
Voc of PV array	64.2 V
MPP Voltage at 25 ◦C Vmpp	54.7 V
MPP Current at 25 ◦C Impp	5.58 A
Temperature coefficient of Voc (%/deg.C)	-0.27269
Temperature coefficient of Isc (%/deg.C)	0.061745
Parallel resistance (Rp)	269.5934Ω
Series resistance (Rs)	0.37152 Ω
Diode ideality factor	0.94504

Simulation inputs for the solar panel model are the incident solar irradiance and the ambient temperature. These parameters are updated at each time interval, and they are subject to the variability of the data. The simulation outputs of the solar panel array at each time step are the current, voltage and power generated. The PV array generates the maximum amount of power at around 100KW within the given irradiation (1000W/m^2,25°C). An R load (constant impedance) model is used to examine the PV system behavior under the FLC MPPT algorithm. Loads in a stand-alone system are commonly categorized into fixed and flexible ones, depending on the comfort choices defined by the user. The simplified R no constant load model consists of a resistor R connected in parallel (R_{L1} & R_{L2}) with values of 30000Ω and 10000Ω respectively. The load profile adopted in this study is as follow:

- ✓ *From 0 to 1.25s : load1* = 30000Ω,
- ✓ *From 1.25 to 2.5s : load1+load2* = 40000Ω,
- ✓ *From 2.5 to 3s : load1* = 30000Ω,

The obtained simulation results are summarized in Figures 11-17. Figure 11 shows the incident solar irradiance and the ambient temperature profile. Figure 12 depicts the PV array voltage $V_{pv}(t)$ (Figure 12(a)) and current $I_{pv}(t)$ (Figure 12(b)) responses, respectively.

The plots of results in Figure 13 show the duty cycle (d), calculated from a conventional FLC MPPT controller, and its effect on the promising performance and accurate tracking of the stand-alone system according to the profile change of irradiance and temperature, this figure also illustrates the DC-DC voltage and current respectively. Figure 13(a) shows the duty cycle temporal evolution calculated from the PWM signal, then Figure 13(b) gives the DC-DC converter voltage and the Figure 13(c) illustrates the currents generated by the DC-DC converter, the mean and the rms currents respectively. Simulation results are obtained as shown in Figure 14, which shows the SOC and current battery. Figure 14(a) shows that the estimate SOC curve follows the measured SOC closely. Therefore, Figure 14(b) depicts the measured and estimated battery current with its *zoomed-in views*. Figure 14 shows clearly how the real SOC reflects precisely the battery operation, whether in charging or discharging mode.

Figure 15 shows the inverter output voltage before filtering, which contains the harmonic components. In addition, we can easily see that the stability of the inverter output voltage is always assured even with the load variation. However, Figure 16 shows the Inverter output *Vabc* Voltage (a) and *RMS(Vabc)* (b) with varying

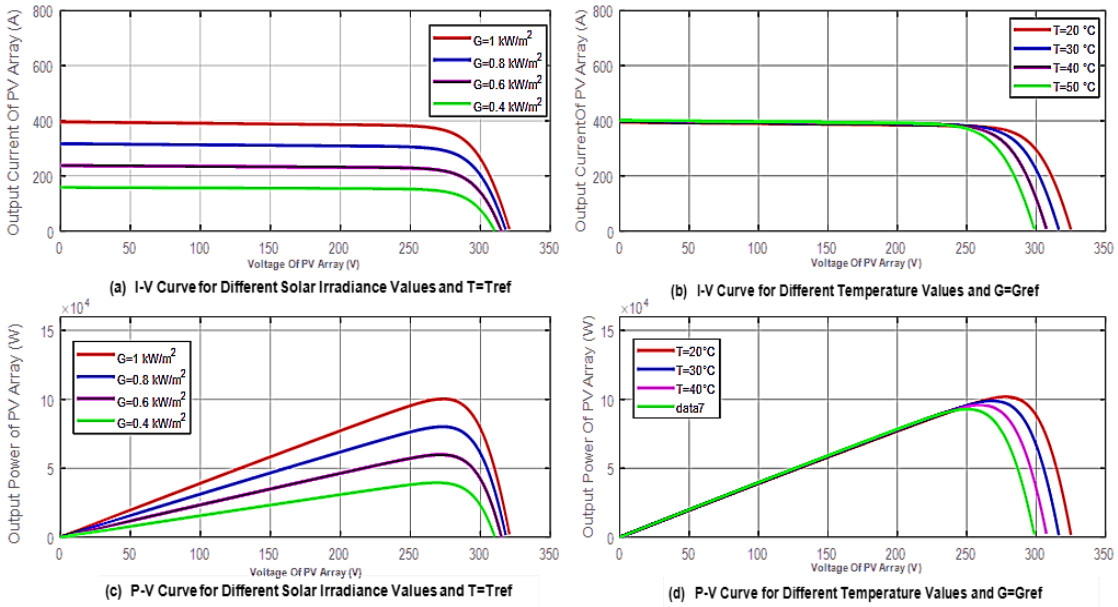

Figure 10. I-V and P-V characteristics of PV array under various temperatures and solar irradiation levels

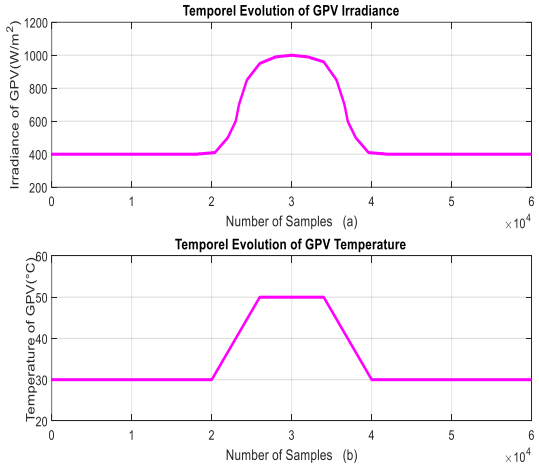

Figure 11. The incident solar irradiance (a) and the ambient temperature (b) profile

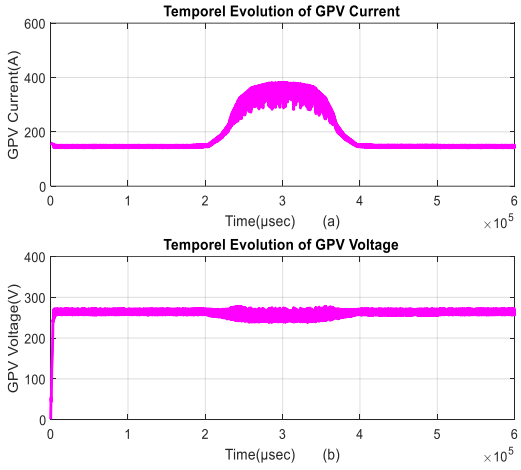

Figure 12. GPV ($\mathbf{I_{pv}}$ & $\mathbf{V_{pv}}$) behavior during sudden full load Temporal Evolution of $\mathbf{I_{pv}}$ (a) and $\mathbf{V_{pv}}$ (b)

irradiance and temperature values with no constant. Then the figure (Figure 17) shows the produced power trajectories for all three stand-alone alone components, PV panels, battery and the load. The main goal of hybrid system management is to satisfy the battery and load needs. For this assumption, the control algorithm starts with the selection of the mode connection, and then it checks the battery SOC, after that it passes to the comparison between the panel power and that required by the load demands. These comparisons are done according to the following main cases:

Case 1: The solar power covers the load demand, and charges the battery banks.

Case 2: The battery helps the PV generator to supply the load demand.

As Figure 17 shows, the PV panel generates the energy according to the given climatic conditions (Irradiation, Temperature). The resulting graphs will be discussed according to time intervals, as follows:

From 0 to $\mathbf{1.8520}$***s:*** During this period, the PV energy is greatere than load demand, and the battery is fully charged.

From* 1.8520*s to* 2.5165*s: The PV energy can't cover the power needs despite the increased load demand. The storage battery delivers the lacking power in order to supply the load.

From* 2.5165*s to* 3*s: During this interval time, the PV energy covers the load power needs. The battery is fully charged and the energy supplied by the battery must be zero.

Case Study 02: variable Irradiance and constant Temperature

Simulations depicted in Figures 18-24 illustrate the case with variable Irradiance, constant Temperature and no constant Load. All the waveforms of these figures illustrate the response of PV array type SunPower SPR-305E-WHT-D. However, we can easily conclude that the PV generator is very sensitive to rapid environmental changes and, it is well known that an irradiance change has a much greater effect on array characteristics than does the temperature change. When the irradiance is changed, the power-voltage characteristic of the PV panel and its MPP are simultaneously reformulated. Therefore, the FLC MPPT controller must track the changed MPP rapidly. Figure 18 presents PV panel inputs, irradiance and ambient temperature fixed at 25°C. The signal is drawn to vary from 1000 W/m^2 to 250 W/m^2 and returns to its initial value until the end. Therefore, the Figure 19 shows the I_{pv} and V_{pv} output PV array. These two parameters have the same behavior then the case_01. Figure 20 gives the duty cycle control signal (Figure 20 (a)) Vdc Voltage (Figure 20(b)) and I_{dc} Current (Figure 20(c)) of the DC-DC converter. The control signal (duty cycle) generates adaptive values within the climatic conditions and no constant load. The Dc voltage is around 640V. The Figure 21 shows the SOC measured and estimated by using the Extended Kalman Filter (EKF). This estimator is adopted to introduce a senseless technique to estimate the storage battery SOC. The figures (Figures 22 and 23) illustrate the three-phase inverter response, currents, voltages and rms value. For the power balance between the PV generator and Battery, we can easily see the efficiency of the proposed strategy control. Figure 24 depicted the behavior of the hybrid stand-alone power systems management against the irradiance variation and no constant load demand.

In conclusion, the rapid changing weather should challenge the MPPT algorithm and it does so. However, the reaction of the MPPT controller is quick; by looking at Figures 20(a) and 20(b) it can be seen how fast the MPPT responds to the irradiance change. At the end of this research work, we can conclude that the obtained results are satisfactory and that the objective to maintain the maximum power possible from a PV generator, during different climatic conditions of the solar insolation and temperature, was realized. This controller makes a shorter time to find the point of maximum power.

The obtained results can be compared with other research works using the same context concerning the power management applied to hybrid systems. In our case, despite the very severe operating conditions, a non-constant load and variable climatic conditions, the proposed controller gives very efficient results compared with those cited in [28, 29]. The chattering phenomenon is damped and the voltage Vdc is almost constant even in the presence of fluctuations during the operating mode. The efficiency of this controller is proven especially during the switching of the power produced by the different sources.

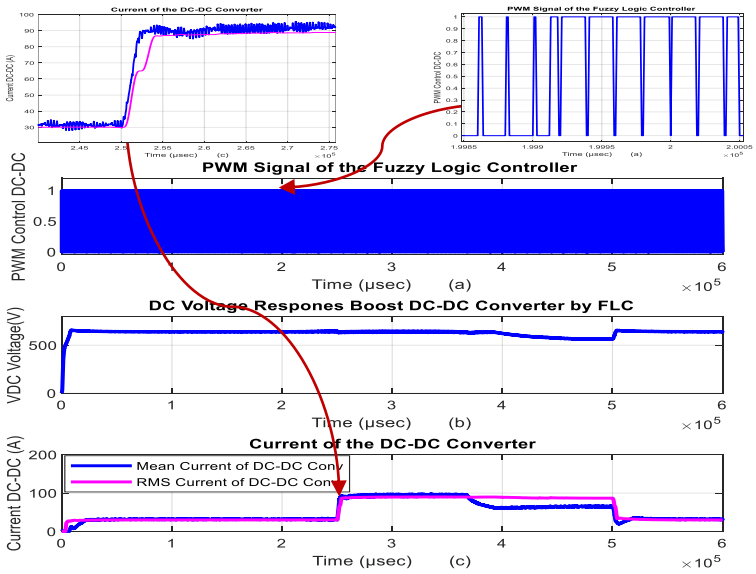

Figure 13. The Cycle duty control signal (a), **Vdc** Voltage (b) and **Idc** Current (c) of the **DC-DC** converter

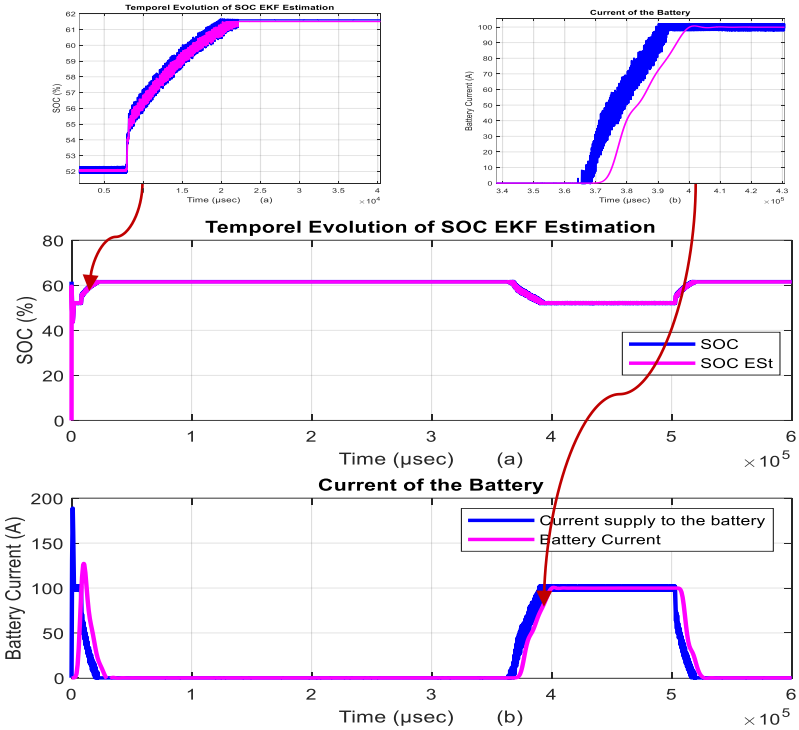

Figure 14. Measurement and Estimate SOC (a), Current supply and generate current (b) of the battery

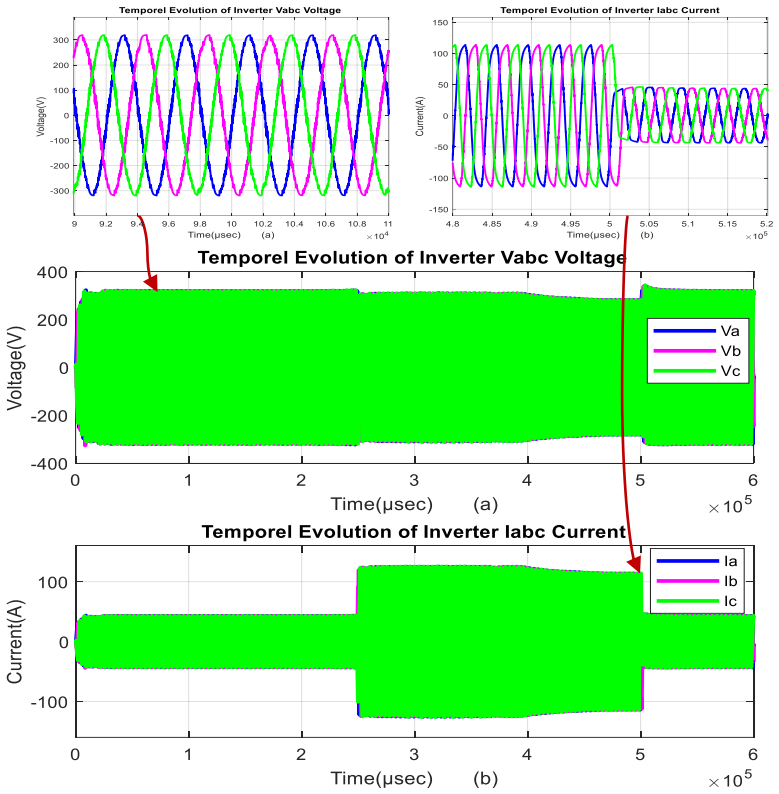

Figure 15. Inverter three phase sinusoidal voltage (a) and current (b) during no constant load according solar irradiance and the ambient temperature condition

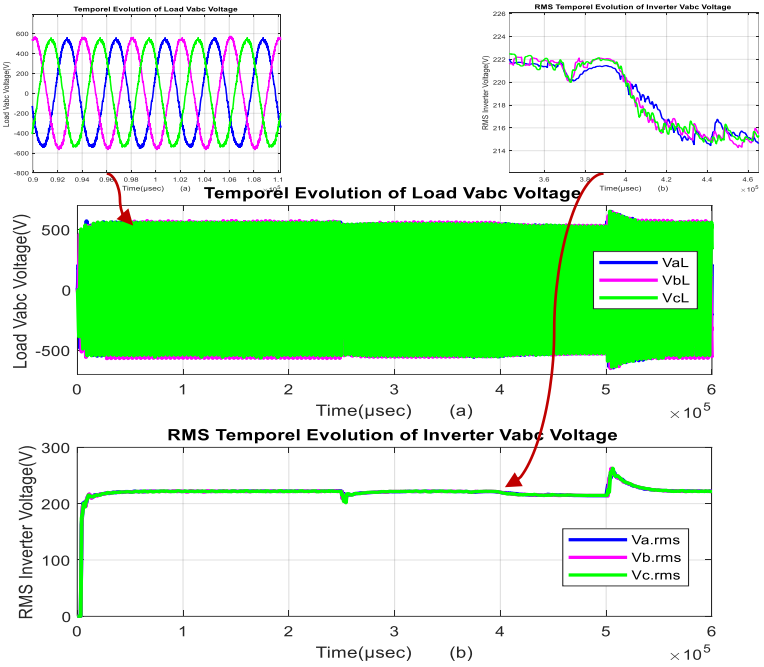

Figure 16. Inverter **Vabc** Phase to Phase Voltage (a) and (b) RMS (**Vabc**) with varying irradiance and temperature values with no constant Load

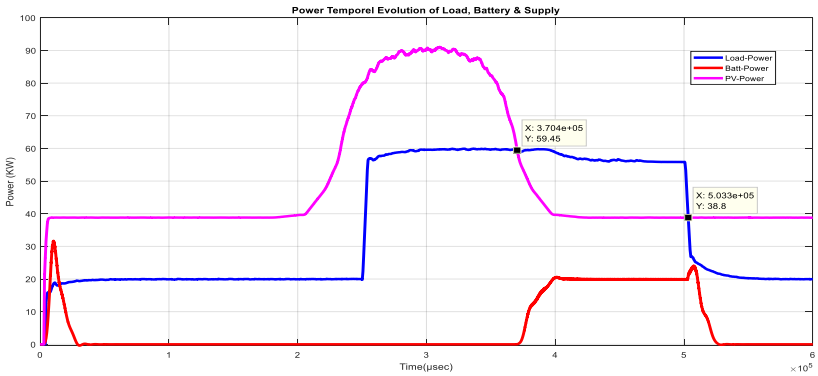

Figure 17. Power balance during integration of PV system and Battery by using a no constant Load

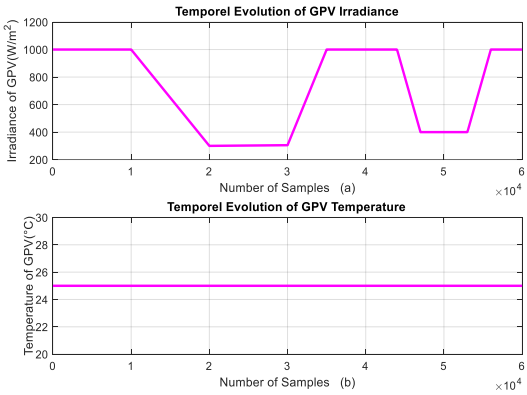

Figure 18. The incident solar irradiance (a) and the ambient temperature (b) profile

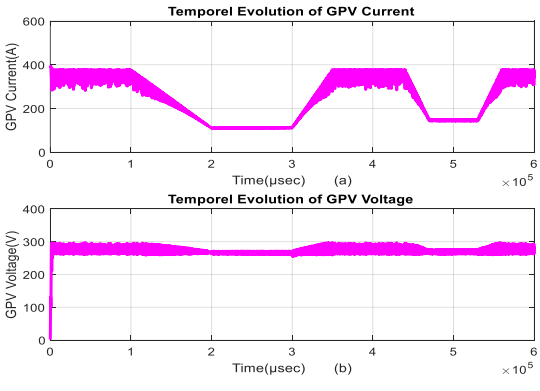

Figure 19. GPV ($\mathbf{I_{pv}}$ & $\mathbf{V_{pv}}$) behavior during sudden full load, temporal evolution of $\mathbf{I_{pv}}$ (a) and $\mathbf{V_{pv}}$ (b)

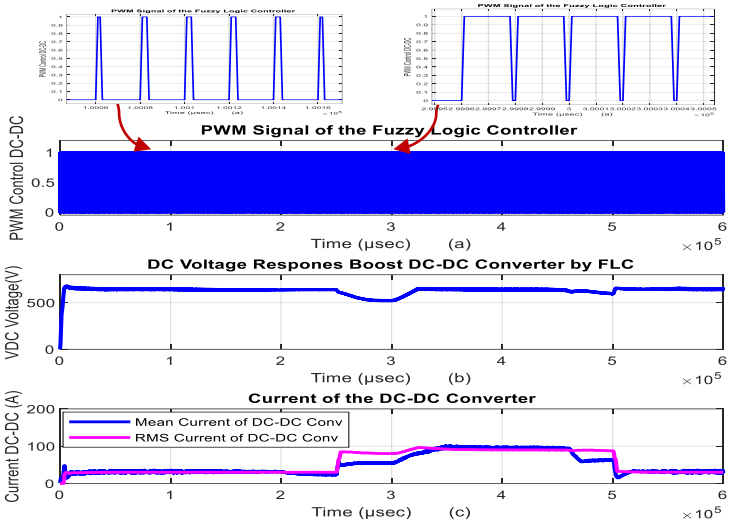

Figure 20. The Cycle duty control signal (a), **Vdc** Voltage (b) and **Idc** Current (c) of the **DC-DC** converter

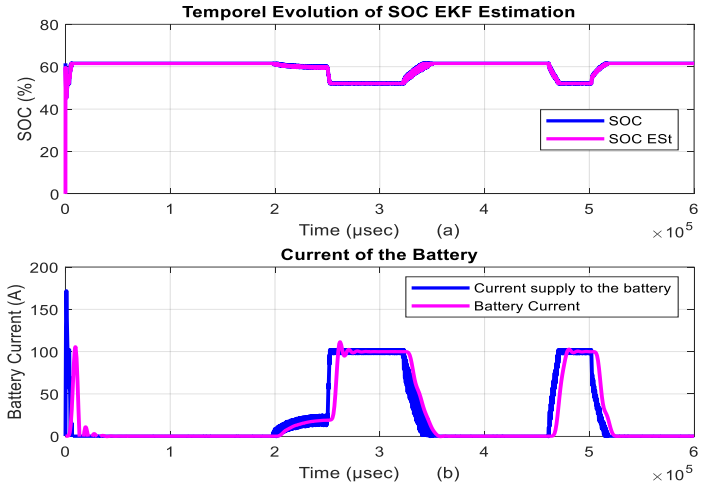

Figure 21. Measurement and Estimate SOC (a), Current supply and generate current (b) of the battery

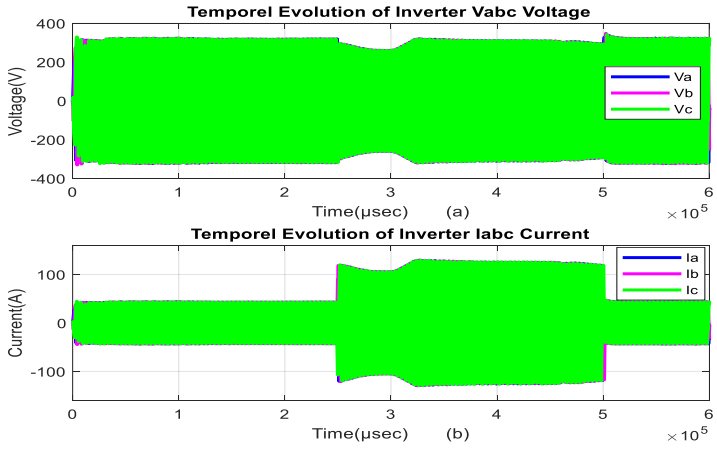

Figure 22. Inverter **Vabc** voltage and current during no constant load according solar irradiance and constant Temperature

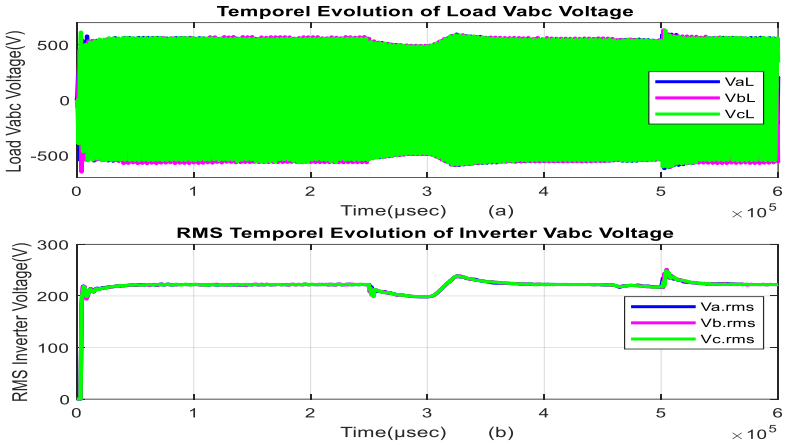

Figure 23. Inverter **Vabc** Phase to Phase Voltage (a) and (b) **RMS(Vabc)** with varying irradiance and temperature values with no constant Load

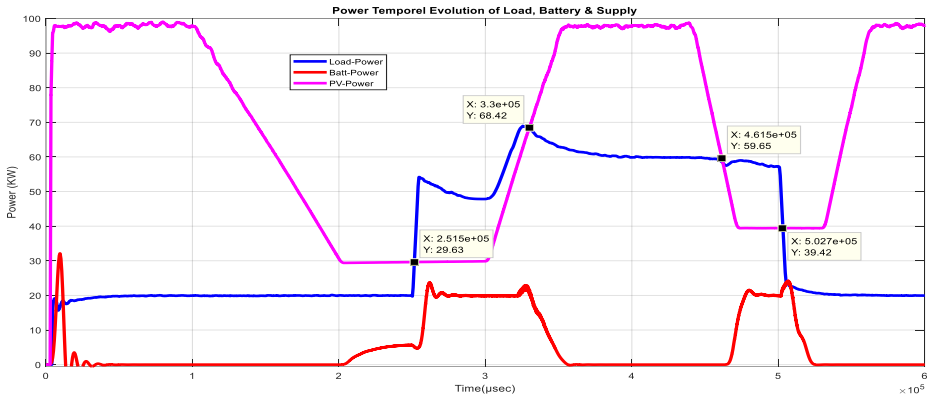

Figure 24. Power balance during integration of PV system and Battery by using a no constant Load

6. CONCLUSION

The purpose of this research work has mainly focused on the development of an autonomous hybrid power system and its energy management unit in variable climatic conditions. To sum up, firstly, the PV array type SunPower SPR-305E-WHT-D is considered in this study, where the developed mathematical model, the boost converter with the FLC MPPT algorithm used to track the given power, the battery charging\discharging, and the EKF algorithm have been explained in deep detail. The fuzzy membership functions are designed based on the triangle method for the fuzzification process and used centroid method for the defuzzification process. The DC-link voltage has been converted to AC voltage by three phase voltage source inverter and applied to no constant load. The EKF algorithm is used to the estimate SOC of a lithium battery pack, with the assumption that the relationship between battery OCV and SOC is piecewise linear and varies with the ambient temperature. The performance of the system at various input conditions is studied with the proposed control. The optimal load sharing has been achieved proportionally among the solar and proper charging and discharging modes of batteries at particular load conditions. The proposed management system conducts to attain the targeted objectives, despite the climatic conditions and load variation, in order to maintain the power demand at satisfactory levels satisfactory and to protect the battery against deep discharging\overcharging. The simulation results show that SOC estimation by using the EKF method is effective and can estimate battery SOC accurately.

7. REFERENCES

1. Necaibia, S., Kelaiaia, M.S., Labar, H., Necaibia, A. and Castronuovo, E.D., "Enhanced auto-scaling incremental conductance mppt method, implemented on low-cost

microcontroller and sepic converter", ***Solar Energy***, Vol. 180, (2019), 152-168. https://doi.org/10.1016/j.solener.2019.01.028

2. Wu, Z., Tazvinga, H. and Xia, X., "Demand side management of photovoltaic-battery hybrid system", ***Applied Energy***, Vol. 148, (2015), 294-304. https://doi.org/10.1016/j.apenergy.2015.03.109
3. Tang, L., Zhang, Y., Xu, W. and Zeng, C., "Novel variable step-size maximum power point tracking control strategy for pv systems based on contingence angles", in 2013 IEEE Energy Conversion Congress and Exposition, IEEE., (2013), 3904-3911.
4. Eldahab, Y.E.A., Saad, N.H. and Zekry, A., "Enhancing the design of battery charging controllers for photovoltaic systems", ***Renewable and Sustainable Energy Reviews***, Vol. 58, (2016), 646-655. https://doi.org/10.1016/j.rser.2015.12.061
5. Jiang, Y., Qahouq, J.A.A. and Haskew, T.A., "Adaptive step size with adaptive-perturbation-frequency digital mppt controller for a single-sensor photovoltaic solar system", ***IEEE Transactions on Power Electronics***, Vol. 28, No. 7, (2012), 3195-3205. doi: 10.1109/TPEL.2012.2220158.
6. Manganiello, P., Ricco, M., Petrone, G., Monmasson, E. and Spagnuolo, G., "Optimization of perturbative pv mppt methods through online system identification", ***IEEE Transactions on Industrial Electronics***, Vol. 61, No. 12, (2014), 6812-6821. doi: 10.1109/TIE.2014.2317143.
7. Deveci, O. and Kasnakoğlu, C., "Performance improvement of a photovoltaic system using a controller redesign based on numerical modeling", ***International Journal of Hydrogen Energy***, Vol. 41, No. 29, (2016), 12634-12649. https://doi.org/10.1016/j.ijhydene.2016.05.149
8. Hassani, H., Zaouche, F., Rekioua, D., Belaid, S., Rekioua, T. and Bacha, S., "Feasibility of a standalone photovoltaic/battery system with hydrogen production", ***Journal of Energy Storage***, Vol. 31, (2020), 101644. https://doi.org/10.1016/j.est.2020.101644
9. Chan, C., Lo, E. and Weixiang, S., "The available capacity computation model based on artificial neural network for lead–acid batteries in electric vehicles", ***Journal of Power Sources***, Vol. 87, No. 1-2, (2000), 201-204. https://doi.org/10.1016/S0378-7753(99)00502-9
10. Zhang, F., Liu, G. and Fang, L., "A battery state of charge estimation method with extended kalman filter", in 2008 IEEE/ASME International Conference on Advanced Intelligent Mechatronics, IEEE., (2008), 1008-1013.
11. Zhang, F., Liu, G. and Fang, L., "A battery state of charge estimation method using sliding mode observer", in 2008 7th world congress on intelligent control and automation, IEEE., (2008), 989-994.
12. Uddin, M.H., Baig, M.A. and Ali, M., "Comparision of 'perturb & observe'and 'incremental conductance', maximum power point tracking algorithms on real environmental conditions", in 2016 International Conference on Computing, Electronic and Electrical Engineering (ICE Cube), IEEE., (2016), 313-317.
13. Sera, D. and Baghzouz, Y., "On the impact of partial shading on pv output power", ***Proceedings of RES'08***, (2008). https://www.researchgate.net/publication/259786752
14. Khelif, M., M'raoui, A. and Malek, A., "Simulation, optimization and performance analysis of an analog, easy to implement, perturb and observe mppt technique to be used in a 1.5 kwp photovoltaic system", in 2013 International Renewable and Sustainable Energy Conference (IRSEC), IEEE. (2013), 10-17.
15. Sera, D., Valentini, M. and Raducu, A., "Real time photovoltaic array simulator for testing grid-connected pv inverters", in 2008 IEEE International Symposium on Industrial Electronics, ISIE 2008, IEEE., (2008).
16. Motahhir, S., Aoune, A., El Ghzizal, A., Sebti, S. and Derouich, A., "Comparison between kalman filter and incremental conductance algorithm for optimizing photovoltaic energy", ***Renewables: Wind, Water, and Solar***, Vol. 4, No. 1, (2017), 1-10. https://doi.org/10.1186/s40807-017-0046-8
17. Aoune, A., Motahhir, S., El Ghzizal, A., Sebti, S. and Derouich, A., "Determination of the maximum power point in a photovoltaic panel using kalman filter on the environment psim", in 2016 International Conference on Information Technology for Organizations Development (IT4OD), IEEE., (2016), 1-4.
18. Vasebi, A., Partovibakhsh, M. and Bathaee, S.M.T., "A novel combined battery model for state-of-charge estimation in lead-acid batteries based on extended kalman filter for hybrid electric vehicle applications", ***Journal of Power Sources***, Vol. 174, No. 1, (2007), 30-40. https://doi.org/10.1016/j.jpowsour.2007.04.011
19. Rahimi Mirazizi, H. and Agha Shafiyi, M., "Evaluating technical requirements to achieve maximum power point in photovoltaic powered z-source inverter", ***International Journal of Engineering, Transactions C: Aspects*** Vol. 31, No. 6, (2018), 921-931. doi: 10.5829/ije. 2018.31.06c.09.
20. Rupesh, M. and Vishwanath, T., "Intelligent controllers to extract maximum power for 10 kw photovoltaic system", ***International Journal of Engineering, Transactions A: Basics*** Vol. 35, No. 4, (2022), 784-793. doi: 10.5829/ije.2022.35.04a.18.
21. Al-Majidi, S.D., Abbod, M.F. and Al-Raweshidy, H.S., "A novel maximum power point tracking technique based on fuzzy logic for photovoltaic systems", ***International Journal of Hydrogen Energy***, Vol. 43, No. 31, (2018), 14158-14171. https://doi.org/10.1016/j.ijhydene.2018.06.002
22. Senthil, R., "Global mppt control algorithms for solar pv systems under non-uniform solar radiation", ***International Journal of Recent Technology and Engineering***, Vol. 7, (2019), 2102-2105.
23. Boutabba, T., Drid, S., Chrifi-Alaoui, L. and Benbouzid, M., "A new implementation of maximum power point tracking based on fuzzy logic algorithm for solar photovoltaic system", ***International Journal of Engineering, Transactions A: Basics*** Vol. 31, No. 4, (2018), 580-587. doi: 10.5829/ije.2018.31.04a.09.
24. Plett, G.L., "Extended kalman filtering for battery management systems of lipb-based hev battery packs: Part 3. State and parameter estimation", ***Journal of power sources***, Vol. 134, No. 2, (2004), 277-292. https://doi.org/10.1016/j.jpowsour.2004.02.033
25. Bhangu, B., Bentley, P., Stone, D. and Bingham, C., "Observer techniques for estimating the state-of-charge and state-of-health of vrlabs for hybrid electric vehicles", in 2005 IEEE Vehicle Power and Propulsion Conference, IEEE., (2005), 780-789,
26. Vikhe, P., Sabale, A., Kadu, C., Mandhare, V. and Jondhale, A., "Pv generation with battery storage supplying a variable load–supervision and control strategy", Vol. 27, No. 12, (2021).
27. Soliman, M.S., Belkhier, Y., Ullah, N., Achour, A., Alharbi, Y.M., Al Alahmadi, A.A., Abeida, H. and Khraisat, Y.S.H., "Supervisory energy management of a hybrid battery/pv/tidal/wind sources integrated in dc-microgrid energy storage system", ***Energy Reports***, Vol. 7, (2021), 7728-7740. https://doi.org/10.1016/j.egyr.2021.11.056
28. Anagreh, Y.N., Alnassan, A. and Radaideh, A., "High performance mppt approach for off-line pv system equipped with storage batteries and electrolyzer", ***International Journal of Renewable Energy Development***, Vol. 10, No. 3, (2021). doi: 10.14710/ijred.2021.34131.

Persian Abstract

چکیده

سیستم های تولید برق مستقل به گونه ای طراحی شده اند که مستقل از شبکه برق عمومی کار کنند. باتری ها عنصر مهم در سیستم PV مستقل را تشکیل می دهند. آنها برای ذخیره برق تولید شده توسط انرژی خورشیدی در یک شب یا برای استفاده اضطراری در طول تقاضای بار غیر ثابت استفاده می شوند. این مقاله دارای سه بخش اصلی است. اولی مربوط به طراحی یک روش هوشمند برای ردیابی نقطه حداکثر توان مبتنی بر کنترل کننده منطق فازی برای بهبود کارایی یک سیستم انرژی خورشیدی مستقل است. بخش دوم وضعیت شارژ باتری (SOC)را توضیح می دهد. مدل پیشنهادی، که پاسخ SOC واقعی باتری لیتیومی را بهتر منعکس می‌کند، با استفاده از تخمین‌گر حالات فیلتر کالمن (EKF)ساخته شده است. این روش پیشنهادی را می توان به عنوان روشی دقیق تر و قابل اعتمادتر برای تخمین وضعیت شارژ باتری در نظر گرفت. بخش سوم یک سیستم مدیریت برای دو منبع انرژی تجدید پذیر فوق را یکپارچه می کند. عملکرد سیستم مدیریت پیشنهادی با استفاده از کنترل‌کننده منطق فازی مبتنی بر ردیابی نقطه حداکثر توان FLC-MPPT و برآوردگر EKF در Matlab/Simulink در تابش خورشیدی و دمای متفاوت برای درخواست انرژی بدون بار ثابت شبیه‌سازی شده‌اند.